Int. J. Rock Mech. Min. Sci. & Geomech. Abstr. Vol. 25, No. 6, pp. 431–437, 1988
Printed in Great Britain

0148-9062/88 $3.00 + 0.00
Pergamon Press plc

Elastic Wave Velocity and Attenuation as Used to Define Phases of Loading and Failure in Coal

V. R. SHEA*
D. R. HANSON*

This paper discusses a procedure used to investigate the behaviour of elastic wave velocity and attenuation as an indicator for changes in load and structural integrity of coal samples. By measuring the changes in compressional(P)- and shear(S)-wave attenuation and velocity under uniaxial and triaxial testing conditions, their effectiveness for distinguishing changes in applied load and structural failure of the sample can be observed. The velocity and attenuation values were used in further calculations such as ratios of P-wave to S-wave attenuation and velocity values, dynamic elastic constants, normalized velocities, and attenuation coefficients to reveal any trends that may exist upon loading and failure.

The behaviour of both P-wave and S-wave attenuation and velocity considered together define distinct and consistent phases of load change and failure under uniaxial and triaxial testing conditions. The S-wave attenuation and velocity are more sensitive than those of the P-wave to changes in axial load and the initial development of microfractures within the sample preceding structural failure. The attenuation and velocity ratio curves and the dynamic elastic constant curves are not very sensitive to changes in load, but are responsive to structural failure of the coal sample. The attenuation coefficient and normalized velocity curves revealed the same trends observable in the original velocity and attenuation curves.

INTRODUCTION

This report describes the results of laboratory work performed as one phase of a U.S. Bureau of Mines research project that investigated non-destructive methods to verify the location of the yielded zone and stress abutment peak in coal mine pillars. The yielded zone refers to an outer envelope of failed and fractured coal defined by Wilson to be peripheral to an abutment zone of high stress within the pillar [1–3]. Measurement of the extent of this zone within the pillar would require a method that is sensitive to both changes in stress and the development of fractures within the coal.

The influence of fractures and change in stress upon attenuation and velocity of ultrasonic elastic waves travelling through a fractured and stressed medium has been well-documented [4–13]. In particular, Su *et al.* [6], Stacey [10], Lockner *et al.* [11], Thill [12], Molina and Wack [13], and Terry [14] obtained experimental results pertinent to the application of elastic wave attenuation and velocity used in this investigation. Stacey [10] determined that shear waves are more responsive than compressional waves to irregularities such as fractures or voids within the rock. Lockner *et al.* [11] proposed that ultrasonic wave attenuation is more sensitive than velocity to the presence of microfractures that form in rock subjected to increasing stress applied perpendicular to the direction of wave propagation prior to failure. Molina and Wack [13] found that the closing of cracks by adding load to a core sample improved the coupling within the rock sample, increasing energy transmission through the sample as well as the velocity of the elastic waves. This trend continued with increasing load until applied stress began to cause the formation of new cracks within the sample, at which point energy transmission decreased. Terry [14], in contrast to the other references, experimented with the effects of compressional waves propagated through coal samples. Terry found that coal contained air filled cracks, which he called "layer cavities," that are oriented parallel to bedding. Test samples were drilled perpendicular to bedding, perpendicular to major cleat, and perpendicular to minor cleat. He found a greater increase of velocity upon initial loading in the samples perpendicular to bedding, indicating that the layer cavities had a more significant effect on velocity than either major or minor cleat.

* Geotechnical Division, Denver Research Center, USBM, P.O. Box 25086, Denver, CO 80225, U.S.A.

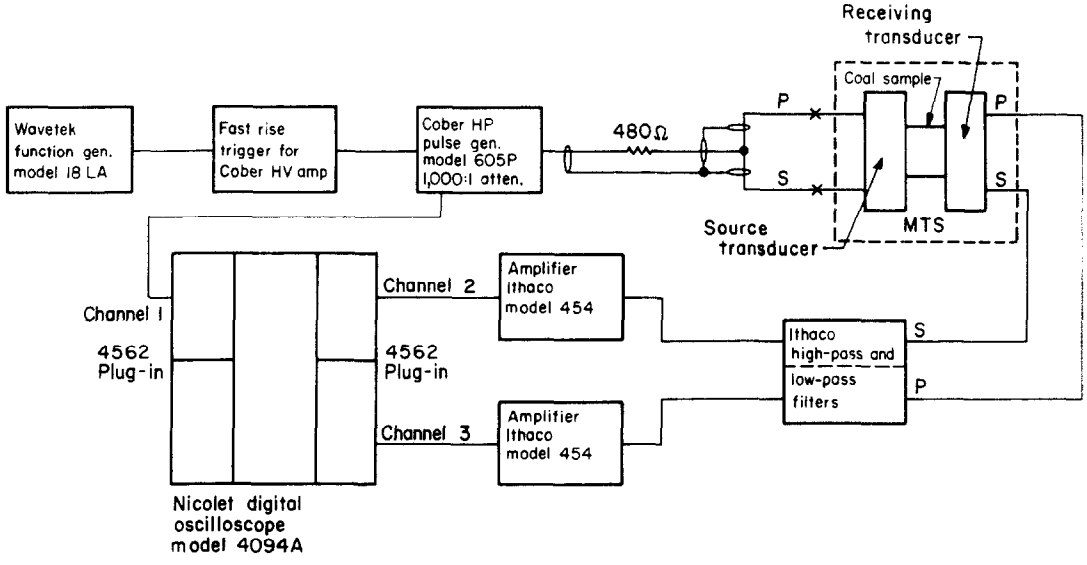

Fig. 1. Schematic diagram of the experimental set-up.

Initial load applied parallel to wave propagation caused a non-linear increase in velocity. Once the layer cavities were closed by load, then the change of velocity was more linear with respect to increase in load. Su *et al.* [6] investigated the effectiveness of compressional wave velocities at measuring the magnitude and direction of stresses surrounding boreholes drilled in sample blocks of rocks to which external stresses were applied. These collective results from previous work lead to the hypothesis for this investigation—that elastic wave velocity and attenuation would be effective for measurement of changes in stress and structural integrity with distance into a coal pillar accessed by a drill hole, and that these laboratory results could be applied to field detection of the stress abutment peak and the yielded zone in a coal pillar.

For this experiment, selected methods described above were employed to monitor the change in the behaviour of P- and S-wave velocity and attenuation in response to increase in load. The testing conditions used in the laboratory experiment were chosen in order to simulate as closely as possible the conditions that would be found in a coal pillar. In a coal pillar, stress is usually oriented perpendicular to bedding. The coal samples to be tested were, therefore, drilled perpendicular to bedding, and were loaded axially to simulate conditions within a coal pillar. The P- and S-waves were also propagated perpendicular to bedding and parallel to the direction of loading. This orientation of loading also provided the advantage that the presence of layer cavities parallel to the bedding in coal causes a greater change in velocity and attenuation of elastic waves upon initial loading.

TEST EQUIPMENT

As shown in Fig. 1, the experimental set-up includes two 1-MHz Harisonic* compressional and shear wave transducers, the first transmitting the source signal through the coal sample, and the second receiving the signal after it has travelled through the coal. A Wavetek function generator supplies a 5 V square wave which triggers a Cober Electronics, Inc., high-power function generator. This pulse drives the source transducer and provides a reference signal from which arrival times can be measured. Ithaco amplifier and band pass filters amplify and filter the signal from the receiving transducer. A four-channel Nicolet model 4094A digital storage oscilloscope displays the source signal on channel one, which serves as a reference, with the second and third channels displaying the P- and S-wave signals, respectively, from the receiving transducer. The coal sample is held in the load frame of a servocontrolled Material Testing System (MTS), which applies an axial load to the coal sample at a controlled rate and allows a given load to be maintained for an interval of time.

The transducers consist of lithium sulfate crystals that transmit and receive both P- and S-waves. Each transducer contains two types of transducer crystals within one casing, with the P-wave crystal being annular, surrounding the centrally located S-wave crystal. A correction factor must be included in attenuation calculations to compensate for signal attenuation caused by the transducers and coupling between the transducers and coal sample. The Cober function generator is necessary to drive a large enough source signal through the coal sample. The signal voltage used for the tests ranges from 500 to 600 V, and the frequency is 1 KHz. The pulse width of the driving signal from the Cober is 47 μsec measured at 90% of average pulse amplitude, with 943 μsec between pulses to allow for damping of all reflections in the sample before the next pulse arrives. The driving signal pulse excites both the P- and S-crystals in the driving transducer simultaneously. Once the signals are input to the Nicolet oscilloscope, the error involved in their measurement is ± 0.25 mV for ampli-

* Reference to specific trade names is made for identification only and does not imply endorsement by the Bureau of Mines.

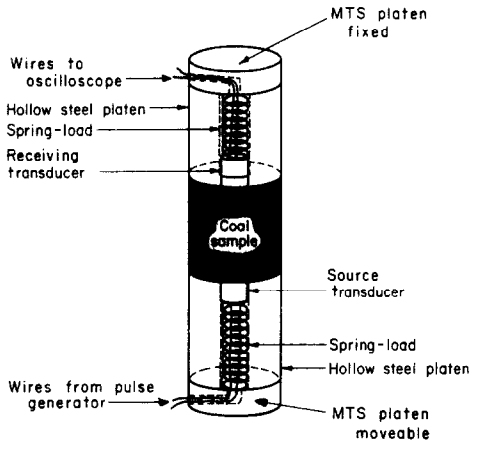

Fig. 2. Coal sample enclosed in steel platens with hollow internal chambers to hold the transducers spring-loaded against the sample at constant pressure.

tude and $\pm 0.25\,\mu$sec for arrival time. The error involved in amplitude measurement leads to an error of ± 0.05 dB in P-wave attenuation values and an error of ± 0.03 dB in S-wave attenuation values (less than 0.1% error). The error involved in the arrival time measurement introduces an error of ± 13 m/sec into P-wave velocity values (approximately 0.5% error) and ± 2.4 m/sec into S-wave velocity (approximately 0.2% error).

EXPERIMENTAL PROCEDURE

Twenty-nine core samples of coal approximately 5.06 cm (1.99 in.) in diameter drilled perpendicular to bedding were weighed, measured, and placed between 10.16 cm (4.00 in.) long steel platens of the same diameter as shown in Fig. 2. The samples ranged from 10.90 to 10.55 cm (4.29 to 4.15 in.) in length with the average being 10.65 cm (4.19 in.) A table of sample data is included in the Appendix. The samples prepared for uniaxial tests were shorter because it was difficult for the signal to travel through a longer, unconfined coal sample. A centred hole 1.56 cm (0.6 in.) in diameter within the platens contained the transducers and the spring-loads which pressed the transducers against the samples at a constant pressure. A steel disc of the same diameter as the platens with the length of 1.78 cm (0.70 in.) was attached to each platen by screws to hold the spring assembly in place. The wires that connected the source transducer to the function generator and receiving transducer to the oscilloscope passed through the centre of the spring coil. A groove in the steel disc accommodated the wires as shown in Fig. 2. To assure good signal transmission between the coal sample and the transducers, a commercially available gel couplant designed for transmission of ultrasonic signals was applied to the transducers. Both uniaxial and triaxial tests were performed on coal samples. For triaxial tests the sample was covered with a neoprene sleeve to isolate it from hydraulic fluid which was used to apply a uniform confinement pressure to the sample. The range of confinement pressure used for the triaxial tests included 1.7, 3.5, 5.2, 6.9 and 8.6 MPa (250, 500, 750, 1000 and 1250 psi, respectively). Throughout the duration of each test, the confinement pressure was held constant within the triaxial load chamber.

The MTS applied an axial load to the sample by displacing the loading head at a fixed rate of 1.7×10^{-3} mm/sec (6.7×10^{-5} in./sec). At axial load increments of 4450 N (1000 lb) for the 4 uniaxial tests and 17,800 N (4000 lb) for the 25 triaxial tests, sample loading was suspended for 3–5 min after each increment to allow for structural stabilization within the sample in response to increased load. At the end of each pause, while load was held constant, three arrival times and their corresponding maximum amplitudes were recorded and averaged for each wave type. P- and S-wave signals were not able to be transmitted through some of the coal samples at zero probably because of the layer cavities oriented parallel to bedding in the coal and perpendicular to signal propagation. The MTS applied load until the sample could no longer support additional load. At this point, the sample was considered to have structurally failed. After sample failure, while the load was removed from the sample, arrival times and amplitude measurements were recorded when there was adequate signal reception through the coal. In a few of the triaxial tests, no signals could be transmitted through the failed sample. During only one uniaxial test were any post-failure measurements possible.

Control of sample unloading was difficult to maintain once the sample had failed. For this reason post-failure data readings were taken at random loads while the sample was being unloaded. Because the sample was failed, it was difficult to maintain a fixed load long enough to take more than one arrival time and amplitude reading for each load.

From the sample length and travel times recorded at each load increment, the velocities of the S-waves and the P-waves were calculated. Axial deformation in response to loading of the sample, was included in each velocity calculation. Attenuation of the signals caused by

Table 1. Equations used in data calculations

Calculations of Dynamic Elastic Constants

Poisson's ratio $= [1/2 - (V_s/V_p)^2]/[1 - (V_s/V_p)^2] = \nu$,
Shear modulus $= \rho V_s^2 = S$ (or G),
Bulk modulus $= \rho[V_p^2 - (4/3)V_s^2] = K$,
Young's modulus $= V_p^2\rho[(1 - 2\nu)(1 + \nu)/(1 - \nu)] = E$,

where

V_p = compressional wave velocity,
V_s = shear wave velocity,
ρ = pre-testing density of coal sample,
ν = Poisson's ratio,
(from Duvall [15]).

Calculation of Attenuation Values

$A = 20$ log (output voltage/input voltage).
$I_x = I[(e^{-ax})/x]$,

where

a = the attenuation coefficient,
I = initial amplitude,
I_x = amplitude at distance x from the source,
(from Dobrin [16]).

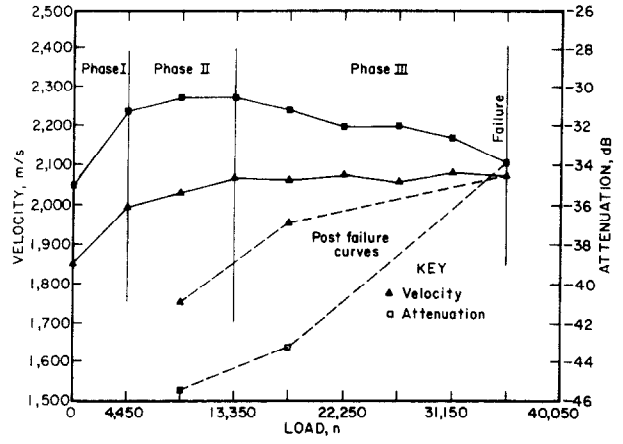

Fig. 3. Velocity and attenuation of the P-wave vs load for a uniaxial test showing the three phases of behaviour change as load increases and as failure occurs.

travel through the coal sample was calculated by comparing the amplitudes of the input and output signals, as shown in the equation in Table 1. In order to compare attenuation values between samples of varying length, the attenuation coefficient was also calculated using the equation in Table 1. From the compressional and shear wave velocities and the density of the coal sample, the dynamic elastic constants were calculated for each load using the equations in Table 1. Ratios of P-wave attenuation to S-wave attenuation and P-wave velocity to S-wave velocity were calculated. The velocity values were normalized by the initial velocity values to evaluate percentage change of velocity with each loading increment. All the parameters were plotted and evaluated to determine whether any trends existed in response to sample loading and failure.

DISCUSSION OF RESULTS

Velocity and attenuation

Figures 3 and 4 show representative trends of velocities and signal attenuation values for P- and S-waves, respectively from a uniaxial test. Figures 5 and 6 show trends for the P- and S-waves, respectively, from a representative triaxial test, confinement pressure of 1.7 MPa (250 psi). As the initial load is applied to the coal sample, there is a high rate of increase in velocity and decrease in attenuation, which is labelled Phase I.

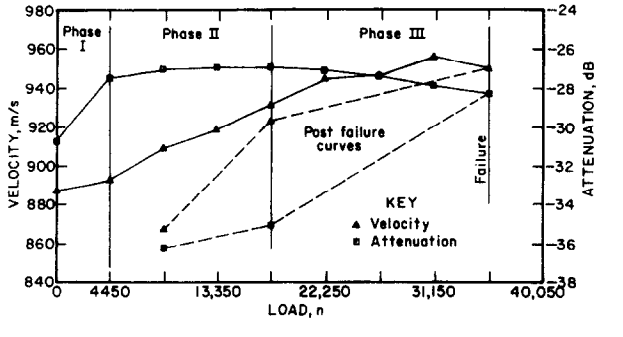

Fig. 4. Velocity and attenuation of the S-wave vs load for a uniaxial test showing the three phases of behaviour change as load increases.

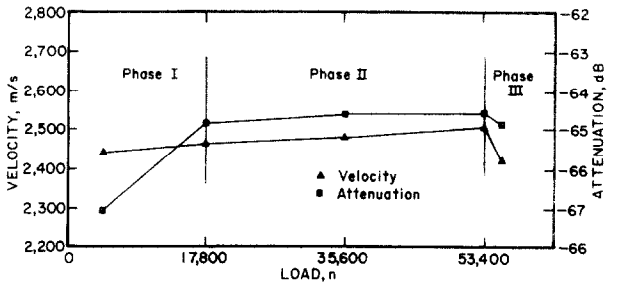

Fig. 5. Velocity and attenuation of the P-wave vs load for a triaxial test showing the three phases of behaviour change as load increases and as failure occurs.

This phase signifies the closing of layer cavities in the coal sample by the initial load, thus allowing the signals to travel more efficiently through the coal with greater velocity and less attenuation. The decline in rate of velocity increase and attenuation decrease is labelled Phase II and indicates that the closing of layer cavities within the coal sample is complete. The linear increase of velocity with respect to increase in load reflects the increase in density caused by elastic compaction of the sample with applied load.

In Phase III the applied load, instead of closing microfractures, appears to be creating microfractures within the coal sample. The presence of microfractures causes an increase in attenuation which is more sensitive to their presence. However, velocity remains fairly constant or increases slightly. Although the microfractures may be developing, they do not impair the ability of the sample to bear load or decrease the velocity of elastic waves travelling through the sample. The change in attenuation behaviour, without a corresponding change in velocity behaviour, indicates that this phase is a transitional one signifying the first stages of failure. The sample is not considered to be failed until it can no longer bear an increase in load or maintain a fixed load. At failure, the changes in velocity and attenuation are abrupt, as shown in the figures.

In general, the P-wave curves do not demonstrate the described phases as consistently as the S-wave curves. The phases are discernible in the uniaxial and triaxial P-wave graphs in Figs 3 and 5, but were not so clear in the majority of the P-waves. The increases in the P-wave velocity with load increase may have been masked by the sampling interval of the oscilloscope (0.5 μsec), which, as discussed earlier, would not detect changes in P-wave velocity of less than 13 m/sec, but would detect changes in the S-wave velocity greater than 2.4 m/sec. At zero load, approximately half the samples subjected to

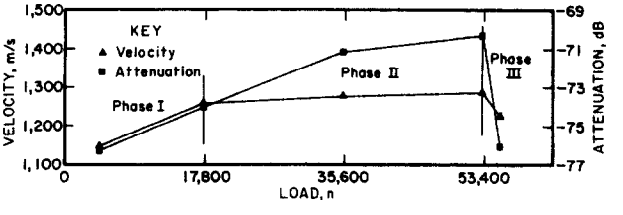

Fig. 6. Velocity and attenuation of the S-wave vs load for a triaxial test showing the three phases of behaviour change under increasing load.

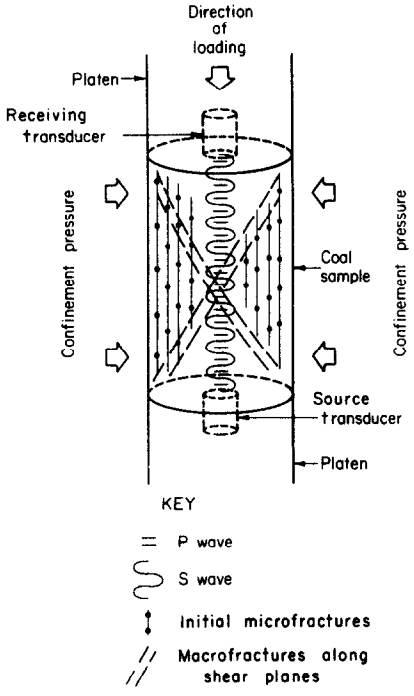

Fig. 7. Illustration of the mode of failure for a coal sample subjected to axial loading. Initially microfractures (oriented parallel to direction of loading) form throughout the sample. Failure occurs when these microfractures coalesce to form macrofractures that concentrate along shear planes within the sample.

confining pressure did not allow transmission of P- or S-waves, as shown in the Appendix. An initial load of 4450 N (1000 lb) to 17,800 N (4000 lb) was required before measurable wave forms were transmitted through the sample. The effect may have been caused by the fact that confinement pressure, which is applied laterally to the sample and parallel to the layer cavities, acted to hold the layer cavities open during the lower load values. Once a large enough axial load was applied, the effect of confining pressure was offset sufficiently to allow closure of the layer cavities. The signals could then be transmitted through the sample.

Mode of failure

According to Paterson [17], the physical behaviour of coal samples loaded axially to failure can be described by three stages. Stage I begins with the initial application of load, during which the deformation is non-linearly elastic with respect to load. The behaviour is due to the closure of pre-existing voids within the coal parallel to bedding. Stage I corresponds to Phase I as defined by the behaviour of wave attenuation and velocity. Stage II begins after the layer cavities within the sample have closed, and elastic deformation behaves linearly with respect to load. Stage II corresponds to Phase II as defined geophysically. Stage III, shown in Fig. 7, begins with the development of microfractures throughout the sample. These microfractures are oriented parallel to the direction of axial loading. The microfractures cause an increase in attenuation, which is more sensitive than velocity to their presence. Phase III ends when microfracturing becomes extensive enough to cause a decrease in velocity. Stage III ends when microfractures coalesce

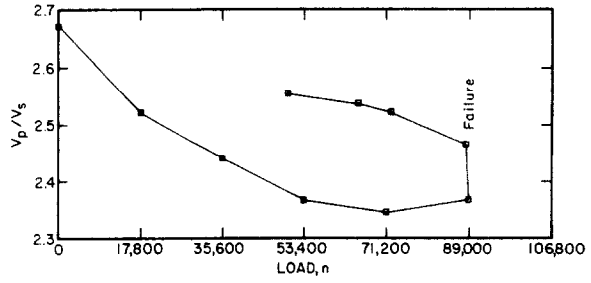

Fig. 8. Ratios of P-wave velocity to S-wave velocity vs load. The ratio decreases initially, indicating that the S-wave velocity increasing with initial load application at a greater rate than the P-wave. After failure the ratio increases, indicating that the S-wave velocity decreases more upon failure than the P-wave.

to form macrofractures, which concentrate along shear planes and lead to sample failure [11, 12, 18, 19]. At this point, there is an abrupt increase in attenuation and decrease in velocity.

Velocity ratios (V_p/V_s)

Because the S-wave is more responsive than the P-wave, the expected trends occur consistently in the plots of velocity ratios. Figure 8 shows a typical plot of V_p/V_s during loading. Initially the ratio decreases as the S-wave velocity increases at a faster rate than the P-wave velocity. Once the load closes the layer cavities within the sample, both P- and S-wave velocities stabilize, as indicated by a flattening of the ratio curve. Then upon failure, a sudden rise in the ratio shows that the S-wave velocity decreases at a greater rate than the P-wave velocity.

Attenuation ratios (A_p/A_s)

The attenuation ratios also consistently demonstrate the expected trends. Figure 9 shows an example of the typical attenuation ratio plot. The ratio increases upon initial loading, stabilizes, then decreases upon failure of the resulting fractures.

Dynamic elastic constants

The dynamic elastic constant values also demonstrate consistent trends. Figure 10 is a graph of Poisson's ratio vs load, and Fig. 11 is a graph of the shear modulus, bulk modulus, and Young's modulus vs load. The values indicate these parameters are insensitive to increase in load, but are responsive to failure. At failure, Poisson's ratio

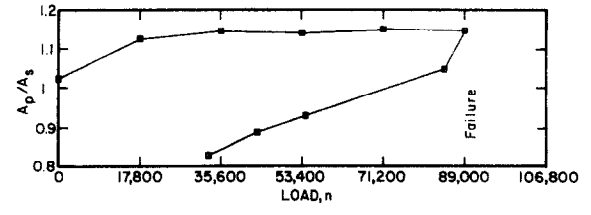

Fig. 9. Ratios of P-wave to S-wave attenuation vs load. The ratio increases initially indicating that the S-wave attenuation decreases more than the P-wave attenuation upon the initial application of load. After failure, the ratio decreases, indicating that the S-wave attenuation increases at a greater rate than the P-wave attenuation upon failure.

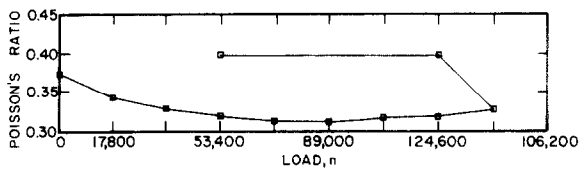

Fig. 10. Poisson's ratio of coal vs load. The ratio remains fairly constant upon loading and increases after failure.

and the bulk modulus increase, while the shear modulus and Young's modulus decrease. Upon sample failure, the limit of elastic deformation is exceeded; therefore, the post-failure numerical values of the dynamic elastic constants are no longer valid. However, the abrupt change in the behaviour of these constants, as shown by the curves, indicates that they are sensitive to failure.

Attenuation coefficients and normalized velocity

The attenuation coefficient curve (not illustrated) is a mirror image of the original attenuation curve about the x-axis. Therefore, the trends illustrated by the original attenuation curve appear in the attenuation coefficient curve, but in inverse form. The points at which attenuation increases, attenuation coefficient decreases, and conversely, where attenuation decreases, attenuation coefficient increases.

Velocity values normalized by the values of velocity at minimum load, illustrates a percentage change of velocity with each load increment. Approximately the same trends observable in the original velocity curves are exhibited in the normalized velocity curves. There is a rapid increase in the normalized velocity values upon initial sample loading, rapid decrease of normalized values upon failure, and a flattening of the normalized velocity curve after initial loading and before failure.

CONCLUSIONS

The conclusions derived from these test results are that shear wave velocity and attenuation are the best parameters of those investigated to distinguish phases of loading and the onset of failure. Dynamic elastic constants, and A_p/A_s and V_p/V_s ratios are valuable only to distinguish between failed and unfailed material and do not appear to be sensitive to changes in load. Attenuation coefficients and normalized velocity values reflect trends illustrated more simply by the original velocity and attenuation curves. It is important to compare the changes in behaviour of velocity and attenuation together in response to loading and failure, so that the previously described phases may be distinguished. Phase III is significant in that it appears to be a phase of structural degradation within the sample that is a precursor to ultimate failure. Molina and Wack [13] correlated the propagation of cracks that accompany failure with the maximum stress with which the sample can be loaded. However, Phase III occurs before the maximum stress is reached, indicating that geophysically detectable microfractures begin to form earlier than the testing methods of Molina and Wack were able to detect. Observation of both attenuation and velocity changes is necessary to detect this phase. Phase III might correspond to the zone adjacent to the interior boundary of the yielded zone of a coal pillar where confinement pressure holds in place material exhibiting incipient fracturing.

The results discussed in this report, supported by the results of previous research in this field, indicate that P-wave and S-wave attenuation and velocity should be effective in detecting the extent of the yield zone and the stress abutment peak within a pillar. Based on laboratory results, probably no signal will be transmittable through the failed material of the yield zone. The inner bounds of the yield zone will probably be detectable by the transmission of the signal through the coal within the pillar. The P- and S-wave velocities and attenuation should then indicate an increase in stress on the coal within the pillar until the stress abutment peak is reached. Moving in toward the centre of the pillar from the stress abutment peak, stress values should decrease, with the decrease being detectable by the change in signal velocity and attenuation. The next step is to test the technique in the field to verify its effectiveness.

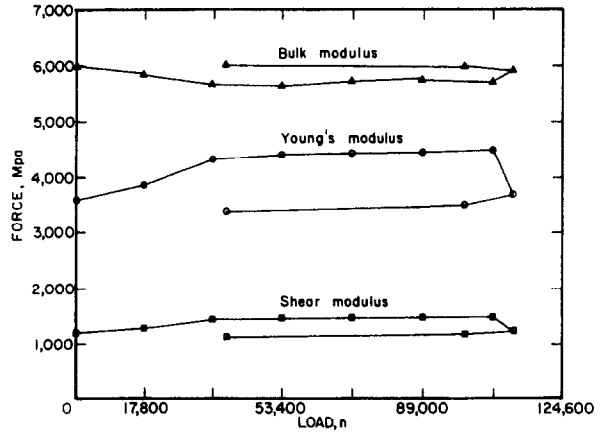

Fig. 11. Bulk modulus, shear modulus, and Young's modulus vs load. These dynamic elastic constants remain fairly constant upon loading. After failure the bulk modulus increases, while the shear modulus and Young's modulus decrease.

Acknowledgements—The authors wish to express their gratitude to Ronald Gerlick, Engineering Technician, Denver Research Center, for his assistance in performing the uniaxial and triaxial testing.

Received 25 *August* 1987; *revised* 2 *June* 1988.

REFERENCES

1. Wilson A. H. Research into the determination of pillar sizes: Part I—an hypothesis concerning pillar stability. *Min. Engr.* **131**, 409–417 (1972).
2. Wilson A. H. The effect of yield zones on the control of ground. *Proc. Sixth Int. Strata Control Conf.*, pp. 1–21. Banff, Canada (1977).
3. Wilson A. H. Stress and stability in coal ribsides. *Proc. First Conf. on Ground Control in Mining*, pp. 1–12. Morgantown, WV (1981).
4. Tatham R. H. Vp/Vs and lithology. *Geophysics* **40**, 336–344 (1982).

5. Hajnal Z., Stauffer M. R., King M. S., Wallis P. F., Wang H. F. and Jones L. E. A. Seismic characteristics of a Precambrian pluton and its adjacent rocks. *Geophysics* **40**, 569–581 (1983).
6. Su W. H., Peng S. S., Okuba S. and Matsuki K. Development of ultrasonic methods for measuring in-situ stresses at great depth. *Min. Sci. Technol.* **1**, 21–42 (1983).
7. Gladwin M. T. Ultrasonic stress monitoring in underground mining. *Int. J. Rock Mech. Min. Sci & Geomech. Abstr.* **19**, 221–228 (1982).
8. Stacey G. P. and Gladwin M. T. Rock mass characterization by velocity and Q measurement. In *Anelasticity in the Earth*, Geodynamics Series 4 (Edited by F. D. Stacey, M. S. Paterson and A. Nicholas) pp. 78–82. AGU (1981).
9. Lin P. and Faulkner G. A sonic wave attenuation technique for monitoring stress levels. *Proc. Fourth Conf. on Ground Control in Mining*, pp. 196–205. Morgantown, WV (1985).
10. Stacey T. R. Seismic assessment of rock masses. *Proc. Symp. on Exploration for Rock Engineering*, pp. 113–117. Johannesburg (1976).
11. Lockner D. A., Walsh J. B. and Byerlee J. D. Changes in seismic velocity and attenuation during deformation of granite. *J. Geophys. Res.* **82**, 5374–5377 (1977).
12. Thill R. E. Acoustic methods for monitoring failure in rock. *Proc. 14th Symp. on Rock Mechanics*, pp. 649–687. University Park, PA (1973).
13. Molina J. P. and Wack B. Crack field characterization. *Int. J. Rock Mech. Min. Sci. & Geomech. Abstr.* **19**, 267–278 (1982).
14. Terry N. B. Dependence of elastic behaviour of coal on microcrack structure. *Fuel* **3**, 125–146 (1959).
15. Duvall W. I. The effect of anisotropy on the determination of dynamic elastic constants of rocks. *Soc. Mech. Engrs. Trans.* **232**, 309–316 (1965).
16. Dobrin M. B. *Introduction to Geophysical Prospecting*, 630pp. McGraw-Hill, New York (1976).
17. Paterson M. S. *Experimental Rock Deformation—The Brittle Field*, 254 pp. Springer-Verlag, New York (1978).
18. Elliot G. M. and Brown E. T. Yield of a soft, high porosity rock. *Géotechnique* **35**, 413–423 (1985).

APPENDIX

Sample No.	Coal seam	Sample length (cm)	Sample density (g/cm^3)	Confinement pressure (psi)	Confinement pressure (MPa)	Load (N) at 1st signal received	Load (N) at failure
U1	Blind Canyon	5.25	1.14	0	0	5340	32,485
U2	Blind Canyon	5.12	1.13	0	0	0	34,265
U3	Blind Canyon	4.91	1.15	0	0	4450	25,365
U4	Blind Canyon	4.81	1.15	0	0	0	59,408
T1	Blind Canyon	10.62	1.17	500	3.5	8900	95,230
T2	Blind Canyon	10.65	1.32	1000	6.9	0	129,050
T3	Blind Canyon	10.63	1.26	250	1.7	4450	63,190
T4	Blind Canyon	10.64	1.36	250	1.7	4450	50,730
T5	Blind Canyon	10.56	1.32	500	3.5	17,800	82,770
T6	Blind Canyon	10.73	1.22	1250	8.6	17,800	135,503
T7	Blind Canyon	10.90	1.22	1000	6.9	17,800	104,130
T8	Blind Canyon	10.66	1.60	1250	8.6	4450	109,470
T9	Blind Canyon	10.64	1.28	750	5.2	0	89,668
T10	Wattis Seam	10.65	1.44	750	5.2	0	89,890
T11	Wattis Seam	10.59	1.29	1000	6.9	17,800	93,005
T12	Wattis Seam	10.66	1.38	1250	8.6	17,800	125,490
T13	Wattis Seam	10.63	1.38	750	5.2	17,800	85,663
T14	Wattis Seam	10.58	1.39	500	3.5	0	92,338
T15	Wattis Seam	10.69	1.38	250	1.7	0	78,765
T16	Wattis Seam	10.70	1.38	500	3.5	0	85,663
T17	Wattis Seam	10.60	1.44	750	5.2	0	64,748
T18	Rock Canyon	10.71	1.30	250	1.7	8900	70,755
T19	Rock Canyon	10.59	1.30	750	5.2	4450	104,798
T20	Rock Canyon	10.59	1.29	1250	8.6	0	151,078
T21	Rock Canyon	10.55	1.29	500	3.5	17,800	102,350
T22	Rock Canyon	10.65	1.30	1250	8.6	0	125,268
T23	Rock Canyon	10.75	1.31	1000	6.9	0	121,485
T24	Rock Canyon	10.69	1.28	250	1.7	17,800	66,083
T25	Rock Canyon	10.58	1.29	1000	6.9	4450	142,845